

Estimating velocities of infectious disease spread through spatio-temporal log-Gaussian Cox point processes

Fernando Rodriguez Avellaneda

Computer, Electrical and Mathematical Sciences and Engineering Division,
King Abdullah University of Science and Technology (KAUST),
Thuwal, Saudi Arabia,

Jorge Mateu

Department of Mathematics,
Universitat Jaume I, Castellon, Spain
and

Paula Moraga

Computer, Electrical and Mathematical Sciences and Engineering Division,
King Abdullah University of Science and Technology (KAUST),
Thuwal, Saudi Arabia

September 10, 2024

Abstract

Understanding the spread of infectious diseases such as COVID-19 is crucial for informed decision-making and resource allocation. A critical component of disease behavior is the velocity with which disease spreads, defined as the rate of change between time and space. In this paper, we propose a spatio-temporal modeling approach to determine the velocities of infectious disease spread. Our approach assumes that the locations and times of people infected can be considered as a spatio-temporal point pattern that arises as a realization of a spatio-temporal log-Gaussian Cox process. The intensity of this process is estimated using fast Bayesian inference by employing the integrated nested Laplace approximation (INLA) and the Stochastic Partial Differential Equations (SPDE) approaches. The velocity is then calculated using finite differences that approximate the derivatives of the intensity function. Finally, the directions and magnitudes of the velocities can be mapped at specific times to examine better the spread of the disease throughout the region. We demonstrate our method by analyzing COVID-19 spread in Cali, Colombia, during the 2020-2021 pandemic.

Keywords: Bayesian inference, Stochastic Partial Differential Equations, Finite differences

1 Introduction

Transmission of infectious diseases such as COVID-19, as we saw in recent years, has the potential to collapse the healthcare system, causing health, societal, and economic problems [Kaye et al., 2020] [Wu et al., 2021]. For that reason, modeling these diseases is critical to understanding how they spread, and this could help decision-makers create policies to mitigate them. In this regard, a powerful tool in the context of spatio-temporal point patterns that can help us understand the spread of an infectious disease is the *velocity* that could be computed given a direction in any location in space and time. This magnitude could be understood as the instantaneous rate of change for the point pattern at location and time (\mathbf{u}, t) in direction \mathbf{v} .

In the context of point patterns, velocity is a quantitative measure that helps us to understand how a spatio-temporal process evolves. Moreover, when it is possible to define the intensity function, velocity refers to how fast the intensity changes in time relative to its change in a given spatial direction. Thus, this measure captures the speed of the intensity change in that direction and provides information about the spatio-temporal dynamics of intensity and, consequently, the underlying point pattern. In this context, velocity could be interpreted in an *instantaneous* sense as the chance for an event to lie in a small product neighborhood of a specific location and time.

Our particular interest concerns the velocity of the spread of contagious diseases over space and time. That means we used the location of infected people by an infectious disease in a particular time resolution, such as days, weeks, or months, and a space window, such as a city or country. With that information, we can define a spatio-temporal point pattern $\{\zeta_i\}_{i=1}^n = \{(\mathbf{u}_i, t_i)\}_{i=1}^n$, with the velocity in a given location \mathbf{u}_0 and time t_0 in the direction \mathbf{v} by the instantaneous relative change for an infected individual in time over the instantaneous change in space in the direction \mathbf{v} . Now, the direction of minimum velocity is associated with the direction of the largest instantaneous change for an event in space. This direction also provides the slowest speed of change in the chance of an event, as explained in Section 3.2.

In this paper, we present how to compute the minimal velocity for infectious diseases. However, a different potential application is using point patterns of species location to

understand the direction and velocity of their movements [Moraga, 2020]. That could help understand their distribution in some specific area related to climate change or other phenomena. Another application is crime data in a given city, which could help us understand how crime changes over time.

Many authors implemented different models to estimate the directional derivatives of the intensity of a point pattern. For instance, [Banerjee and Gelfand, 2003] introduced a formal directional derivative process based on the realization of a stochastic process. Later, [Terres and Gelfand, 2016] developed a methodology for local sensitivity analysis based on directional derivatives that also uses continuous covariates to relate them with spatial gradients. For geostatistical data, temporal and spatial derivatives were computed to estimate velocities of climate change [Schliep et al., 2015] relating covariates to this, for example, temperature. Extending these ideas to point patterns [Schliep and Gelfand, 2019] compute velocities for spatio-temporal point patterns, assuming that the point pattern follows a log-Gaussian Cox (LGCP) process and also by using Nearest Neighbor Gaussian process (NNGP). Additionally, other authors consider other ways to compute velocities that use higher-order derivatives, such as second-order derivatives [Quick et al., 2015].

The main contribution of this paper is computing the minimal velocity using finite differences to approximate partial derivatives of the intensity function. The principal advantage is that we are not using a parametric form of the intensity function or a closed form of the covariance structure. This gives more flexibility to the intensity function, which is an LGCP as in [Schliep and Gelfand, 2019], but we are not fixing the smoothing parameter. This procedure also allows us to capture instantaneous changes that parametric models are slow to capture over time. For the computational part, we use the integrated nested Laplace approximation (INLA) [Rue et al., 2009] that provides computational efficiency to compute the parameters of the parameters of the intensity function.

The structure of the remainder of the paper is as follows. In Section 2, we introduce some theory about point processes and the log-Gaussian Cox process. Then, in Section 3, we fully detail how we decompose the intensity function into three components and how the inference for the LGPC is defined by its covariance structure. In this section, we also explain how velocity is defined for spatio-temporal point patterns and how to approximate it using

finite differences. In Section 4, we present a simulation study to analyze the performance of our method using a point pattern with a deterministic intensity function. Then, in Section 5, we present an application using data from COVID-19 in Cali, Colombia. Finally, in Section 6, we present some conclusions, a discussion of the findings, and some directions for future research.

2 Preliminary concepts

In this section, we first present some theoretical concepts related to point processes necessary to introduce the methodology used to model the spread of disease, and to compute velocities. Using these concepts, we can provide a detailed explanation of how the spread of disease can be modeled both spatially and temporally. This involves analyzing the locations of infected individuals as they change over time. By tracking these observed locations over a specific period, we can gain valuable insights into the patterns and dynamics of disease transmission. This approach allows us to understand where the infections occur and how they evolve, which is crucial for effective disease control and prevention.

2.1 Point processes

Given a subset $W \subseteq \mathbb{R}^2$ and an interval $T \subseteq \mathbb{R}$, a spatio-temporal point pattern consists of a collection of all points $\{\zeta_i\}_{i=1}^n = \{(\mathbf{u}_i, t_i)\}_{i=1}^n \subseteq W \times T$. Under these conditions, a spatio-temporal point process is a random mechanism whose outcome or realization is a point pattern. For a spatio-temporal point process we define the intensity function $\lambda : W \times T \rightarrow [0, \infty)$ such that $\int_A \int_B \lambda(\mathbf{u}, t) dt d\mathbf{u} < \infty$ for all bounded sets $A \subseteq \mathbb{U}$, and intervals $B \subseteq \mathbb{T}$ that satisfies the following property

$$\mathbb{E}[\mathcal{N}(A, B)] = \int_A \int_B \lambda(\mathbf{u}, t) dt d\mathbf{u},$$

where $\mathcal{N}(A, B)$ is the number of points in the region A in the time interval B . Note that we assume that T is an interval in \mathbb{R} , but we will often have $T \subseteq \mathbb{Z}$. In this scenario, we can consider the event times t_i as marks of a spatial point pattern with location \mathbf{u}_i .

One of the most important point processes is the Poisson process. This process is frequently used due to its simplicity, and satisfies the following conditions.

1. For any bounded sets $A \subseteq \mathbb{R}^2$, and interval $B \subseteq \mathbb{R}$, the number of points in the region A in the interval B , $\mathcal{N}(A, B)$ follows a Poisson distribution with mean $\int_A \int_B \lambda(\mathbf{u}, t) dt d\mathbf{u}$.
2. For any bounded set A , any interval B and any $n \in \mathbb{N}$, conditional on $\mathcal{N}(A, B) = n$, the n events in $W \times T$ constitute an independent random sample drawn from the distribution over $W \times T$, which is characterized by the density function

$$f(\mathbf{u}, t) = \frac{\lambda(\mathbf{u}, t)}{\int_W \int_T \lambda(\mathbf{u}, t) dt d\mathbf{u}}.$$

A Poisson process is described by its intensity function $\lambda(\mathbf{u}, t)$, and when this function is constant over the space-time domain, the process is homogeneous. Otherwise, the process is inhomogeneous.

2.2 Log-Gaussian Cox processes

Log-Gaussian Cox processes (LGCPs) are typically used to model complex relationships between space and time, such as the spread of a contiguous disease [Diggle et al., 2013]. To understand this complex process, we start by discussing the Cox process. A Cox process can be viewed as a Poisson process with a random intensity function. That is, the intensity function $\Lambda(\mathbf{u}, t)$ meets these two postulates

1. $\Lambda(\mathbf{u}, t)$ with $\mathbf{u} \in W$ and $t \in T$ is a non negative valued stochastic process,
2. Conditional on the realization $\Lambda(\mathbf{u}, t) = \lambda(\mathbf{u}, t)$ with $\mathbf{u} \in W$ and $t \in T$, the point process is an inhomogeneous Poisson process with intensity $\lambda(\mathbf{u}, t)$.

LGCP models were introduced as a particular case of a Cox process [Møller et al., 1998]. As the name suggests, an LGCP is a Cox process with intensity function given by a Gaussian process, that is $\log(\Lambda(\mathbf{u}, t)) = \mu(\mathbf{u}, t) + \xi(\mathbf{u}, t)$, where $\exp(\mu(\mathbf{u}, t))$ could be interpreted as the mean structure of $\Lambda(\mathbf{u}, t)$ and $\xi(\mathbf{u}, t)$ is a stationary Gaussian process.

3 Methodology

To estimate velocities of an infectious disease, we propose a spatio-temporal point process model to describe how infectious diseases spread in space across time. Specifically, we use a LGCP model where the intensity is multiplicatively decomposed into temporal, spatial, and spatio-temporal stochastic variation as presented in [Diggle et al., 2005] and [Ribeiro Amaral et al., 2023]. Once the model is fitted, the intensity estimate is used to compute *minimal velocities* through finite differences. This approach allows us to understand the direction and velocity of disease spread.

3.1 Spatio-temporal LGCP model

The intensity function of a spatio-temporal LGCP model can be decomposed into three components, namely, a temporal component $\mu(t)$, a spatial component $\eta(\mathbf{u})$, and a spatio-temporal stochastic variation $\xi(\mathbf{u}, t)$. This decomposition is represented as follows

$$\Lambda(\mathbf{u}, t) = \eta(\mathbf{u}) \cdot \mu(t) \cdot \xi(\mathbf{u}, t). \tag{1}$$

Here, the spatial and temporal components are deterministic and capture aspects of the underlying population at risk of the pattern of disease. The spatial component $\eta(\mathbf{u})$ represents the population density in the study region. This implies that if there were zones or locations with higher or lower cases, this variation would be absorbed in $\eta(\mathbf{u})$. The temporal component $\mu(t)$ is estimated by grouping the total number of cases over time, and using a spline model with different basis functions to model this data. Thus, the flexibility of the splines estimation of $\mu(t)$ could capture the anomaly in the number of cases across time. This emphasizes that the remaining term $\xi(\mathbf{u}, t)$ will capture anomalies in space and time. This term is modeled as a stationary, zero-mean log-Gaussian stochastic process. In the following sections, we explain in detail how we compute each component and their importance in the model.

3.1.1 Temporal component

The first step in our approach is to model the number of individuals per temporal unit (e.g., days, hours, etc.) infected by the disease. Accurately capturing this data is crucial for understanding the spread and making reliable predictions. We employed a spline model, a flexible statistical tool capable of fitting complex data patterns to achieve this goal.

Splines allow us to handle non-linear trends in the data, providing a more precise fit than traditional linear models [Wood, 2017]. This flexibility is essential in epidemiological studies, where the number of infections can vary greatly due to numerous factors such as periodic changes due to day-of-week effects or time-of-year events. We, therefore, estimate the number of infected people in time t , denoted by $\mu(t)$ by fitting the following standard log-spline model

$$\log(\mu(t)) = \sum_{i=1}^q \beta_i b_i(t),$$

where b_i are completely known functions, commonly referred to as basis functions and q denotes the number of functions. Some examples of these basic functions are polynomials, roots, cosine, sine, and step functions. However, the election of the basic functions and their number highly depends on the data.

3.1.2 Spatial component

The main objective of this component is to approximate population density. This component is crucial for understanding the patterns of spread of an infectious disease because it directly influences how infections propagate through different regions. High-population-density areas may experience faster and more intense outbreaks due to the increased likelihood of contact between individuals.

Different methods could be used to compute the population density $\eta(\mathbf{u})$ over a study region. In this work, we use population information from WorldPop [Bondarenko et al., 2020], an open-access project that combines official census information and satellite images to estimate population density at different resolutions. For regions where population information is not available, we could estimate the population density using nonparametric methods such as Gaussian kernel estimators [González and Moraga, 2023]. For instance,

the population density could be estimated as

$$\widehat{\eta}(\mathbf{u}) = \left(\frac{1}{n}\right) \sum_{i=1}^n \left(\frac{1}{h^2}\right) \phi\left(\frac{\mathbf{u} - \mathbf{u}_i}{h}\right), \quad (2)$$

where $h > 0$ is a fixed bandwidth, $\phi(\mathbf{u}) = (2\pi)^{-1} \exp\{-0.5\|\mathbf{u}\|^2\}$, and u_i are the location of the infected individuals in the study region across time. We could also use an adaptive bandwidth h_i for each location \mathbf{u}_i to have a better approximation.

3.1.3 Spatio-temporal component

Once the spatial and temporal components are estimated, they can be used to compute the intensity function of the spatio-temporal process. In this case, we assume that the observed point process is generated by a log-Gaussian Cox process. Then, the counting number of infected individuals in the region W at the interval time T called $\mathcal{N}(W, T)$ meets the following conditions

$$\mathcal{N}(W, T) | \Lambda(\mathbf{u}, t) = \lambda(\mathbf{u}, t) \sim \text{Poisson} \left(\int_W \int_T \lambda(\mathbf{u}, t) dt d\mathbf{u} \right),$$

and the intensity function described in Equation (3) could be transformed as

$$\Lambda(\mathbf{u}, t) = \eta(\mathbf{u}) \cdot \mu(t) \cdot \exp(\zeta(\mathbf{u}, t)). \quad (3)$$

Here, $\zeta(\mathbf{u}, t)$ is a stationary Gaussian process with mean $\mathbb{E}(\zeta(\mathbf{u}, t)) = \beta$, that could be conveniently re-parameterized as $\zeta(\mathbf{u}, t) = \beta + \vartheta(\mathbf{u}, t)$ where $\vartheta(\mathbf{u}, t)$ follows a zero-mean Gaussian distribution with a separable covariance structure that is temporally AR1 dependent and spatially dependent with a Matérn covariance function [Matérn, 1960], defined as:

$$\text{Cov}(\vartheta(\mathbf{u}_1, t_1), \vartheta(\mathbf{u}_2, t_2)) = \phi(h_1, h_2) = \sigma^2 \rho(h_1, h_2). \quad (4)$$

Here, $h_1 = \|\mathbf{u}_1 - \mathbf{u}_2\|_2$, $h_2 = |t_1 - t_2|$ and σ represents the spatio-temporal variance. In summary, the covariance function $\rho(h_1, h_2)$ could be defined as

$$\rho(h_1, h_2) = \rho_1(h_1)\rho_2(h_2) = \left[\frac{1}{2^{\nu-1}\Gamma(\nu)} (\kappa \cdot h_1)^\nu \mathbf{K}_\nu(\kappa \cdot h_1) \right] \left[\frac{a^{h_2}}{1 - a^2} \right], \quad (5)$$

where ν is a fixed parameter, $|a| < 1$ and κ are unknown parameters, Γ is the gamma function and \mathbf{K}_ν is the second-order modified Bessel function. The differentiability of the Gaussian process $\vartheta(\mathbf{u}, t)$ depends on the differentiability of the covariance structure; therefore, to ensure this property, we fixed a parameter $\nu \geq 3/2$.

3.1.4 Inference

In summary, the intensity function that models the infected individuals at time t in the spatial window is defined as follows

$$\begin{aligned}\Lambda(\mathbf{u}, t) &= \eta(\mathbf{u}) \cdot \mu(t) \cdot \exp(\zeta(\mathbf{u}, t)), \\ \zeta(\mathbf{u}, t|\theta) &\sim \text{Gaussian Process}(\beta, \phi(h_1, h_2|\theta)), \\ \theta &\sim \text{priors},\end{aligned}$$

where ϕ is the covariance function defined in Equations (4) and (5), and θ is a vector of parameters and hyperparameters.

To fit the model, we use the R-INLA package [Rue et al., 2009] by employing a finite basis function defined on a triangulated mesh of the region of study to approximate the SPDE model in this mesh [Simpson et al., 2015]. This approach introduces a finite-dimensional, continuously specified random field of the form

$$Z(\mathbf{u}, t) = \sum_{i=1}^n z_i \varphi(\mathbf{u}, t),$$

where $\mathbf{z} = (z_1, \dots, z_n)^t$ is a multivariate Gaussian random vector and $\{\varphi(\mathbf{u}, t)\}_{i=1}^n$ is a set of linearly independent deterministic basis functions.

3.2 Velocities

With the intensity function of the underlying LGCP that governs an infectious disease, we can compute the *minimum velocity*. This velocity comes from the advection-diffuse equation used to model the evolution of an implicit function $\psi(\mathbf{u}, t)$ in a specific domain. That is,

$$\frac{\partial \psi(\mathbf{u}, t)}{\partial t} + \mathcal{S}(\mathbf{u}, t) \cdot \nabla \psi(\mathbf{u}, t) = 0, \quad (6)$$

where $\nabla\psi(\mathbf{u}, t)$ is the spatial gradient of the function ψ and \mathcal{S} is the velocity that controls the direction and speed of the function ψ . These functions in the two dimensional spatial case, $\mathbf{u} = (x, y)$ can be written explicitly as

$$\nabla\psi(\mathbf{u}, t) = \begin{pmatrix} \frac{\partial\psi(\mathbf{u}, t)}{\partial x} \\ \frac{\partial\psi(\mathbf{u}, t)}{\partial y} \end{pmatrix}, \quad \mathcal{S}(\mathbf{u}, t) = (\mathcal{S}_x(\mathbf{u}, t), \mathcal{S}_y(\mathbf{u}, t)).$$

The velocity component can also be decomposed as $\mathcal{S}(\mathbf{u}, t) = s_{\mathbf{v}}(\mathbf{u}, t)\mathbf{v}(\mathbf{u}, t)$ where \mathbf{v} is a unit vector that represents the direction of the velocity and $s_{\mathbf{v}}$ is its magnitude in the direction \mathbf{v} . Under these assumptions Equation (6) can be rewritten as

$$\frac{\partial\psi(\mathbf{u}, t)}{\partial t} + s_{\mathbf{v}}(\mathbf{u}, t)[\mathbf{v}(\mathbf{u}, t) \cdot \nabla\psi(\mathbf{u}, t)] = 0. \quad (7)$$

Now, for a fixed velocity direction \mathbf{v} and for a known function ψ we can solve Equation (7) for the magnitude $s_{\mathbf{v}}$ that is always positive, then

$$s_{\mathbf{v}}(\mathbf{u}, t) = \frac{|\partial\psi(\mathbf{u}, t)/\partial t|}{|\mathbf{v}(\mathbf{u}, v) \cdot \nabla\psi(\mathbf{u}, t)|}. \quad (8)$$

Notice that the denominator in Equation (8) is the absolute value of the spatial directional derivative of the function ψ in the direction \mathbf{v} , i.e. $D_{\mathbf{v}}\psi(\mathbf{u}, t) = \mathbf{v}(\mathbf{u}, v) \cdot \nabla\psi(\mathbf{u}, t)$. Then, using Cauchy-Schwartz inequality, we know that the denominator will be bounded by the norm of the spatial gradient, $|\mathbf{v}(\mathbf{u}, v) \cdot \nabla\psi(\mathbf{u}, t)| \leq \|\nabla\psi(\mathbf{u}, t)\|$. Therefore, the largest instantaneous change of the function ψ in a neighborhood of (\mathbf{u}, t) is $\|\nabla\psi(\mathbf{u}, t)\|$ and is in the direction $\mathbf{v}_{\max} = \nabla\psi(\mathbf{u}, t)/\|\nabla\psi(\mathbf{u}, t)\|$. As a result, and because the bounded value is the denominator, the direction \mathbf{v}_{\max} also provides the direction of minimum velocity at (\mathbf{u}, t) that now could be written as

$$s_{\min}(\mathbf{u}, t) = \frac{|\partial\psi(\mathbf{u}, t)/\partial t|}{\|\nabla\psi(\mathbf{u}, t)\|}. \quad (9)$$

In the point process context, following a similar procedure for the intensity function $\lambda(\mathbf{u}, t)$ of a spatio-temporal point process, the direction of minimum velocity captures the

slowest speed of change in intensity in a product neighborhood of (\mathbf{u}, t) . That is, the velocity that provides the slowest speed of change in chance for an event at (\mathbf{u}, t) is

$$s_{\min}(\mathbf{u}, t) = \frac{|\partial\lambda(\mathbf{u}, t)/\partial t|}{\|\nabla\lambda(\mathbf{u}, t)\|}. \quad (10)$$

3.2.1 Computing velocities

We estimate the minimal velocity $s_{\min}(\mathbf{u}, t)$ using the output of the model described in Section 3.1.4 which provides the estimated intensity function $\hat{\lambda}(\mathbf{u}, t)$ over a spatio-temporal grid.

Let Δ_t , Δ_x , Δ_y denote the discrete step size in time t , latitude x and longitude y respectively, and let $\hat{\lambda}(i, j, n)$ be the estimated intensity function in the grid indexed in space for (i, j) and time n . Then, the derivative of the intensity in time that appears in the numerator of $s_{\min}(\mathbf{u}, t)$ can be approximated using numerical methods, such as the *symmetric difference quotient*

$$\frac{\partial\hat{\lambda}(\mathbf{u}, t)}{\partial t} \approx \frac{\hat{\lambda}(i, j, n+1) - \hat{\lambda}(i, j, n-1)}{2\Delta_t}. \quad (11)$$

Notice that the temporal derivative approximation presented in Equation (11) needs future values in time. However, if we are interested in predictions, we can use a first-order divided difference if we do not have access to this value.

To estimate the denominator $\|\nabla\lambda(\mathbf{u}, t)\|$, following [Sethian, 1999], we first define the forward and backward difference operators in space as follows

$$\begin{aligned} D^{+x}\hat{\lambda}(i, j, n) &= \frac{\hat{\lambda}(i+1, j, n) - \hat{\lambda}(i, j, n)}{\Delta_x}, \\ D^{-x}\hat{\lambda}(i, j, n) &= \frac{\hat{\lambda}(i, j, n) - \hat{\lambda}(i-1, j, n)}{\Delta_x}, \\ D^{+y}\hat{\lambda}(i, j, n) &= \frac{\hat{\lambda}(i, j+1, n) - \hat{\lambda}(i, j, n)}{\Delta_y}, \\ D^{-y}\hat{\lambda}(i, j, n) &= \frac{\hat{\lambda}(i, j, n) - \hat{\lambda}(i, j-1, n)}{\Delta_y}. \end{aligned}$$

Here, the positive exponent represents the forward differencing, and the negative represents the backward differencing. Then, using these values, we define the following differential

operators in space

$$\begin{aligned}\|\nabla_1 \hat{\lambda}(i, j, n)\| &= \left((D^{+x} \hat{\lambda}(i, j, n))^2 + (D^{+y} \hat{\lambda}(i, j, n))^2 \right)^{1/2}, \\ \|\nabla_2 \hat{\lambda}(i, j, n)\| &= \left((D^{+x} \hat{\lambda}(i, j, n))^2 + (D^{-y} \hat{\lambda}(i, j, n))^2 \right)^{1/2}, \\ \|\nabla_3 \hat{\lambda}(i, j, n)\| &= \left((D^{-x} \hat{\lambda}(i, j, n))^2 + (D^{+y} \hat{\lambda}(i, j, n))^2 \right)^{1/2}, \\ \|\nabla_4 \hat{\lambda}(i, j, n)\| &= \left((D^{-x} \hat{\lambda}(i, j, n))^2 + (D^{-y} \hat{\lambda}(i, j, n))^2 \right)^{1/2}.\end{aligned}$$

An approximation of the norm of the spatial gradient is then obtained as the average the last four expressions

$$\|\nabla \hat{\lambda}(\mathbf{u}, t)\| \approx \left(\frac{1}{4} \right) \sum_{k=1}^4 \|\nabla_k \hat{\lambda}(i, j, n)\|. \quad (12)$$

Finally, the minimal velocity described in Equation (10) can be approximated using the approximations described in Equations (12) and (11) as follows

$$s_{\min}(\mathbf{u}, t) \approx \frac{\left| \frac{\hat{\lambda}(i, j, n+1) - \hat{\lambda}(i, j, n-1)}{2\Delta_t} \right|}{\left(\frac{1}{4} \right) \sum_{k=1}^4 \|\nabla_k \hat{\lambda}(i, j, n)\|}. \quad (13)$$

4 Simulations

We perform a simulation study to assess the performance of our model in comparison with an underlying truth intensity function. Specifically, we consider a deterministic intensity function to generate a spatio-temporal point pattern in the unit cube, $(\mathbf{u}, t) \in [0, 1]^3$, defined by

$$\lambda(\mathbf{u}, t) = \lambda_0 \exp\{\beta_0 + (1-t)\beta_1 f_1(\mathbf{u}) + t(1-t)\beta_2 f_2(\mathbf{u}) + t^2\beta_3 f_3(\mathbf{u})\}, \quad (14)$$

where each $f_k(\mathbf{u})$ denotes a bivariate normal density with mean $\boldsymbol{\mu}_k$ and covariance matrix Σ_k for $k = 1, 2, 3$, and $\lambda_0 > 0$ is a scaling parameter.

This intensity function, proposed by [Schliep and Gelfand, 2019], was chosen because its close form allows us to compute partial derivatives in space and time, and with that, we can compute the true minimal velocity described in Equation (10).

The partial derivatives of this intensity function has the following form

$$\begin{aligned}\frac{\partial \lambda(x, y, t)}{\partial x} &= \lambda(x, y, t) [(1-t)\beta_1 f_{1x}(x, y) + t(1-t)\beta_2 f_{2x}(x, y) + t^2\beta_3 f_{3x}], \\ \frac{\partial \lambda(x, y, t)}{\partial y} &= \lambda(x, y, t) [(1-t)\beta_1 f_{1y}(x, y) + t(1-t)\beta_2 f_{2y}(x, y) + t^2\beta_3 f_{3y}], \\ \frac{\partial \lambda(x, y, t)}{\partial t} &= \lambda(x, y, t) [-\beta_1 f_1(x, y) + (1-2t)\beta_2 f_2(x, y) + 2t\beta_3 f_3],\end{aligned}$$

where for $k = 1, 2, 3$, f_{kx} denotes the partial derivative in the x direction of f_k and have the following closed form

$$\begin{aligned}f_{kx}(x, y) &= \frac{\partial f_k(x, y)}{\partial x} \\ &= f_k(x, y) \left(-(x - \mu_{k1})\Sigma_{k,11}^{-1} - (y - \mu_{k2})\Sigma_{k,12}^{-1} \right),\end{aligned}$$

and $\Sigma_{k,ij}^{-1}$ is the i th row and j th column of Σ_k^{-1} . Analogously, the partial derivative of the density function f_k in the direction y is

$$\begin{aligned}f_{ky}(x, y) &= \frac{\partial f_k(x, y)}{\partial y} \\ &= f_k(x, y) \left(-(x - \mu_{k1})\Sigma_{k,12}^{-1} - (y - \mu_{k2})\Sigma_{k,22}^{-1} \right).\end{aligned}$$

To simulate the spatio-temporal point pattern, we fixed the parameters as $\lambda_0 = 100$, $\beta_0 = -1.5$, $\beta_1 = 8.0$, $\beta_2 = 2.0$, $\beta_3 = 2.0$, $\mu_1 = (0.4, 0.2)$, $\mu_2 = (0.8, 0.5)$, $\mu_3 = (0.2, 0.8)$, and

$$\Sigma_1 = \begin{pmatrix} 0.065 & -0.030 \\ -0.030 & 0.065 \end{pmatrix}, \Sigma_2 = \begin{pmatrix} 0.065 & 0.000 \\ 0.000 & 0.065 \end{pmatrix}, \Sigma_3 = \begin{pmatrix} 0.065 & 0.030 \\ 0.030 & 0.065 \end{pmatrix}.$$

With these fixed parameters, we use the R package `spatstat` [Baddeley et al., 2015] to generate a realization of an inhomogeneous Poisson process with intensity function given by Equation (14) that generates 7840 points distributed in a grid of temporal resolution of $1/20$ and spatial resolution of $1/30$. These parameters were chosen to show spatio-temporal variability in the intensity function such that the process starts with a mode in μ_1 , for $t \in (0.0, 0.5)$ the mode will move from μ_1 to μ_2 , and for $t \in (0.5, 1)$ the mode will move from μ_2 to μ_3 to finally finish with a mode in μ_3 . In Figure 1, we can see how the mode of the intensity function varies in time points 0, 0.25, 0.5, 0.75, and 1.

Figure 2 compares the true intensity function and the posterior mean generated by the model at time points 0.225, 0.575, and 0.875. As expected, the model captures the

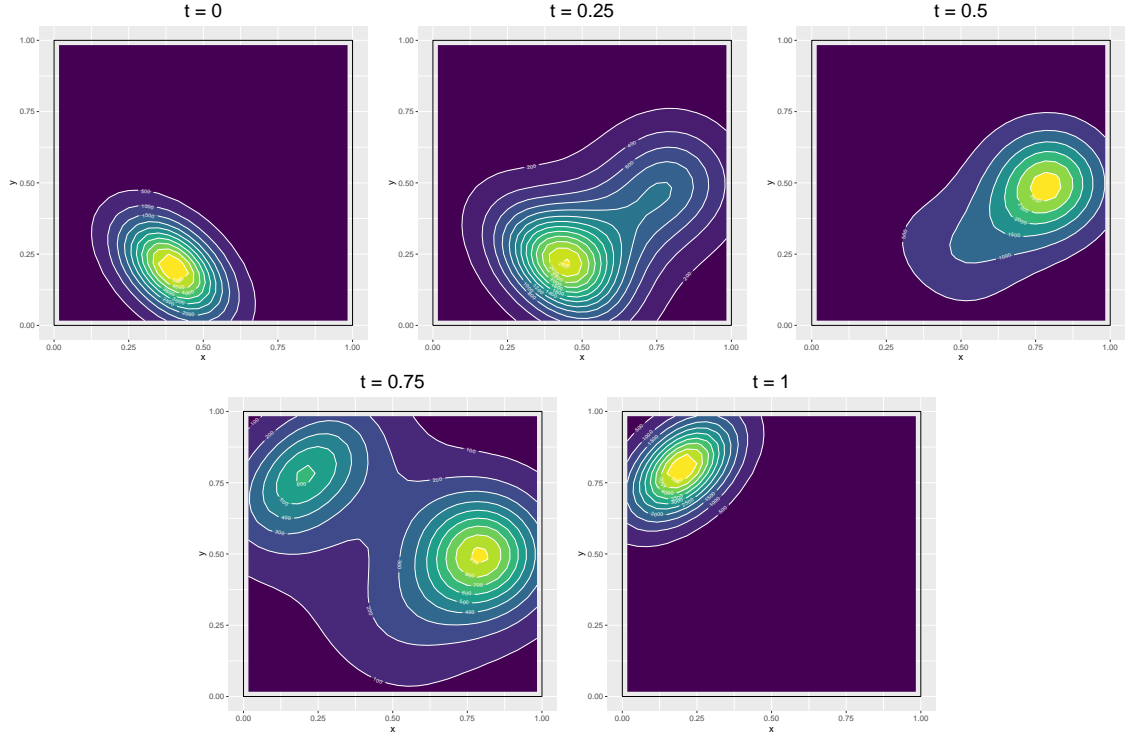
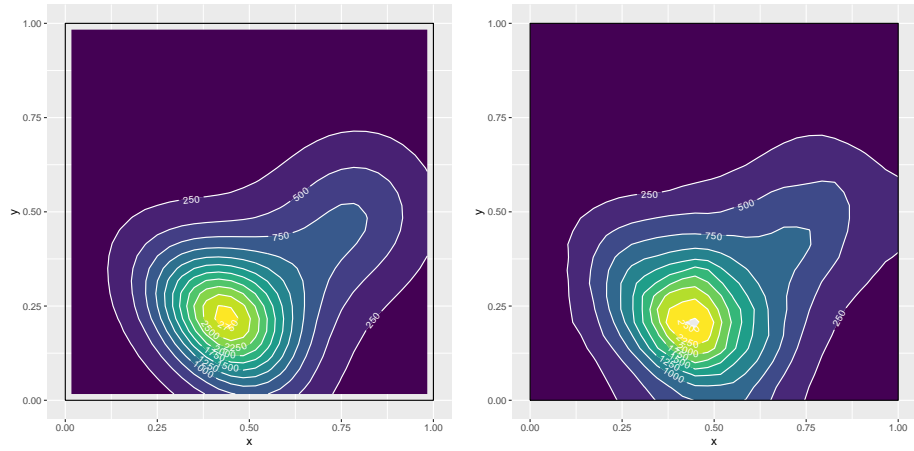


Figure 1: Variation of the intensity in times 0, 0.25, 0.5, 0.75, and 1.

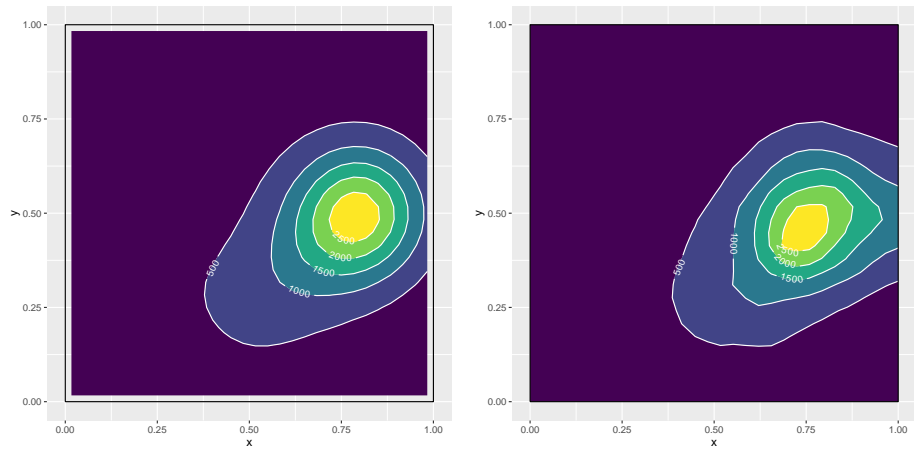
movement of the intensity mode across time. Moreover, we can see that the posterior mean differs slightly from the true values near the boundaries. This happens mainly because the boundaries were artificially defined in the unit cube. However, in general, we can see that the model effectively captures the overall changes in intensity across time.

True and computed spatial and temporal derivatives at time $t = 0.225$ are shown in Figure 3. For computing temporal derivatives in times 0.225 and 0.575, we use a step size of $\Delta_t = 0.2$. When $t = 0.875$, we use a smaller step size of $\Delta_t = 0.1$ in time because the spatio-temporal point process is defined in time in the interval $[0, 1]$. Similarly, true and approximation of the intensity partial derivatives for times 0.575 and 0.875 are shown in Figures 4 and 5. Overall, we can see that the approximation using finite differences captures the trend, maximum, and minimum values of the true values.

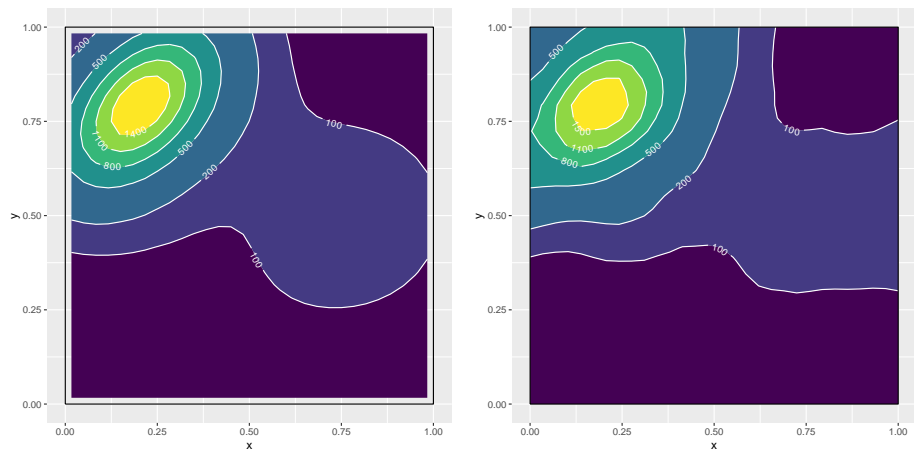
Using the partial derivatives computed before and the gradient approximation described in Equation (12), we can approximate the minimum velocity of the spatio-temporal point process using Equation (13). The true minimum velocity and its approximation for times 0.225, 0.575, and 0.875 are shown in Figure 6. In this figure, the arrows are the standardized



(a) $t = 0.225$

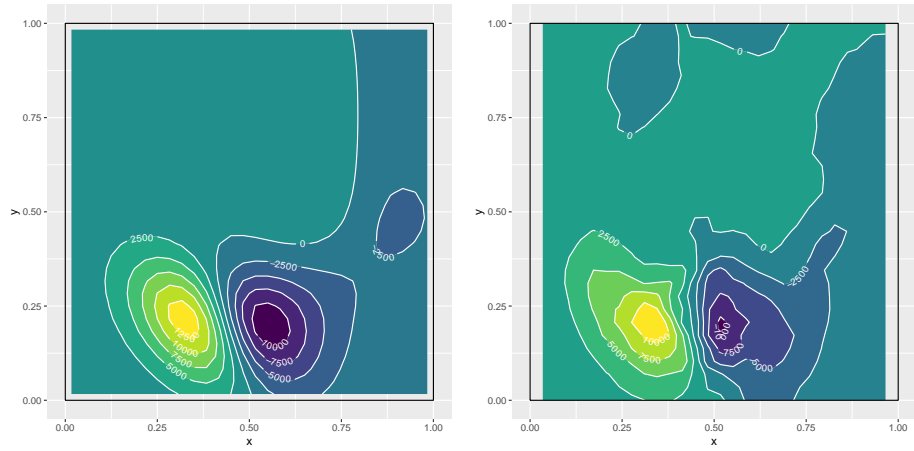


(b) $t = 0.575$

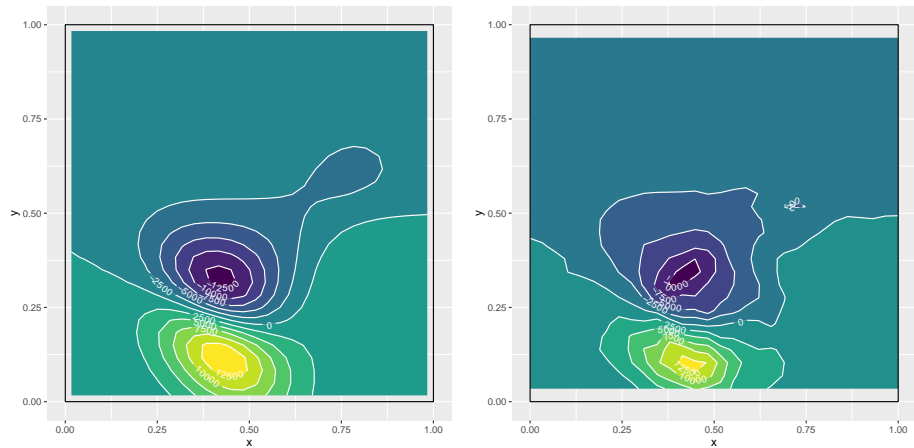


(c) $t = 0.875$

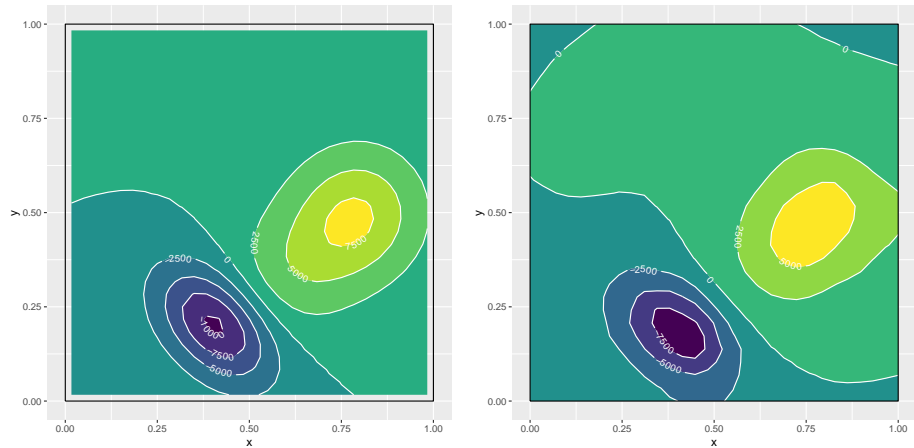
Figure 2: True intensity function (left) and posterior mean (right) for the time points $t = 0.225$, $t = 0.575$ and $t = 0.875$.



(a) $\frac{\partial \lambda(\mathbf{u}, t)}{\partial x}$

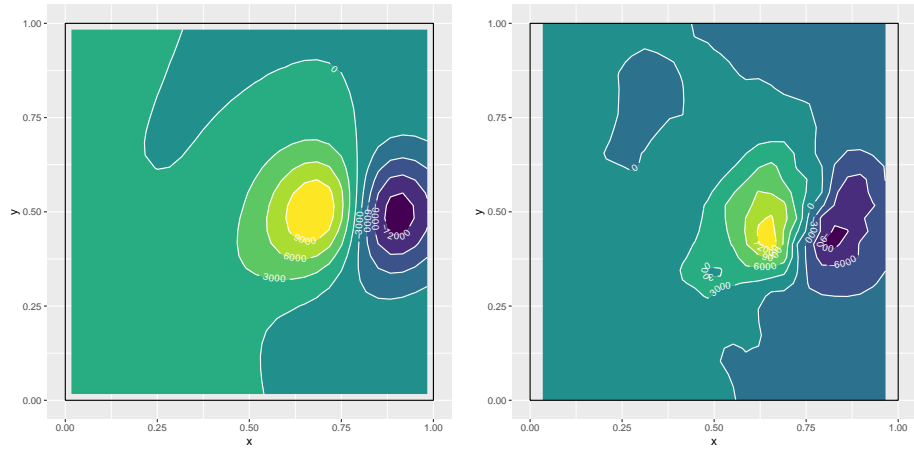


(b) $\frac{\partial \lambda(\mathbf{u}, t)}{\partial y}$

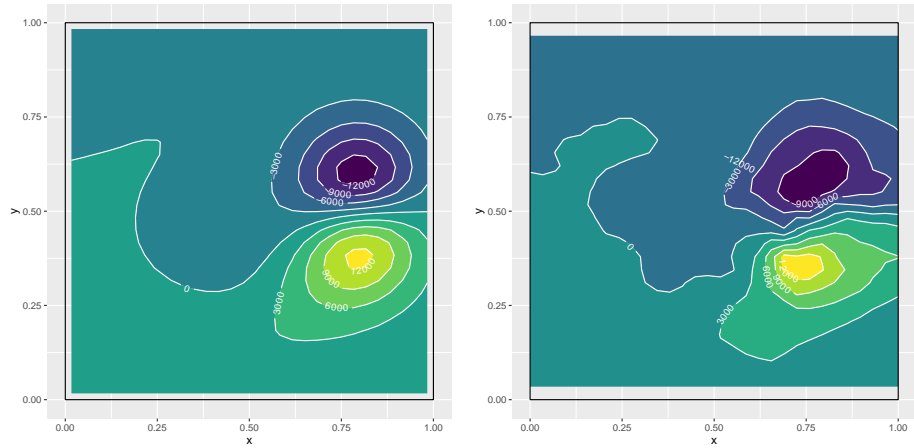


(c) $\frac{\partial \lambda(\mathbf{u}, t)}{\partial t}$

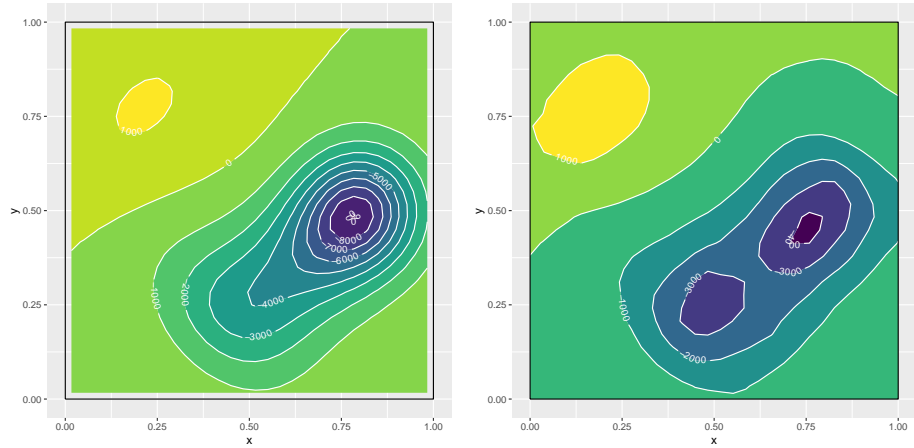
Figure 3: True partial derivatives of the intensity function (left) and finite differences estimation of the partial derivatives (right) at $t = 0.225$



(a) $\frac{\partial \lambda(\mathbf{u}, t)}{\partial x}$

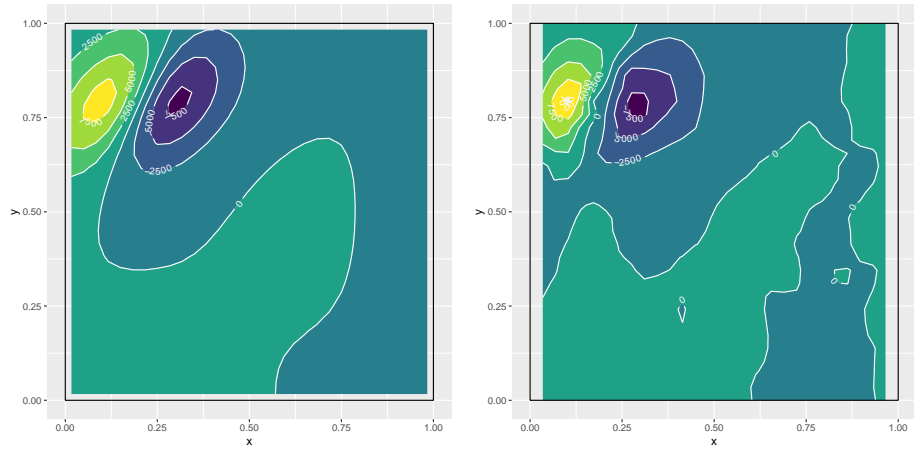


(b) $\frac{\partial \lambda(\mathbf{u}, t)}{\partial y}$

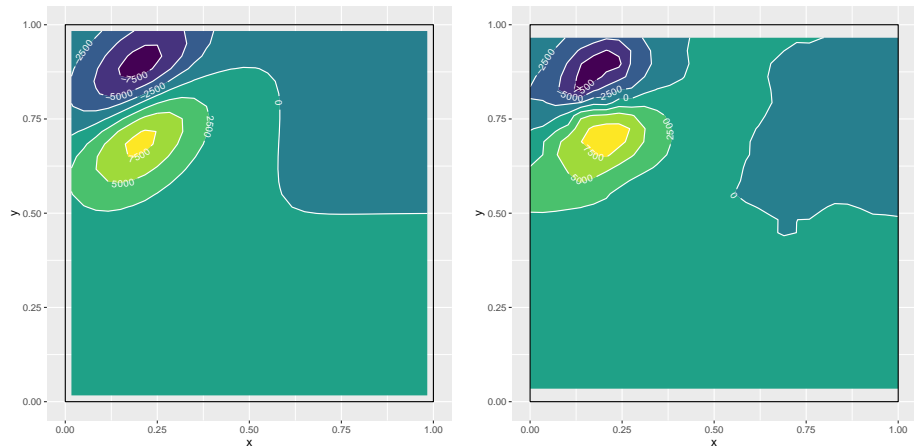


(c) $\frac{\partial \lambda(\mathbf{u}, t)}{\partial t}$

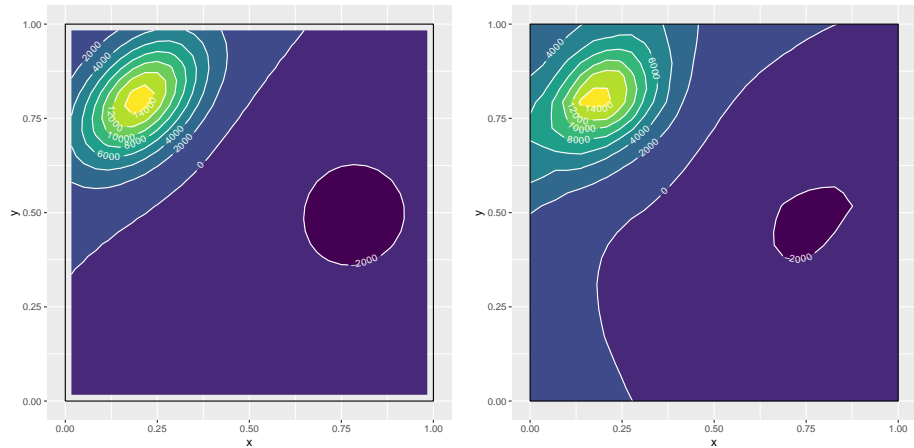
Figure 4: True partial derivatives of the intensity function (left) and finite differences estimation of the partial derivatives (right) at $t = 0.575$



(a) $\frac{\partial \lambda(\mathbf{u}, t)}{\partial x}$



(b) $\frac{\partial \lambda(\mathbf{u}, t)}{\partial y}$



(c) $\frac{\partial \lambda(\mathbf{u}, t)}{\partial t}$

Figure 5: True partial derivatives of the intensity function (left) and finite differences estimation of the partial derivatives (right) at $t = 0.875$

vector that shows the direction in which the slowest speed of change in the intensity is obtained and its positive, i.e.,

$$\vec{s} = \text{sign} \left(\frac{\partial \lambda(\mathbf{u}, t)}{\partial t} \right) \cdot \frac{\nabla \psi(\mathbf{u}, t)}{\|\nabla \psi(\mathbf{u}, t)\|}, \quad (15)$$

where the sign is a function that is -1 if the number is negative, 0 if it is zero, or $+1$ if it is positive.

5 Application

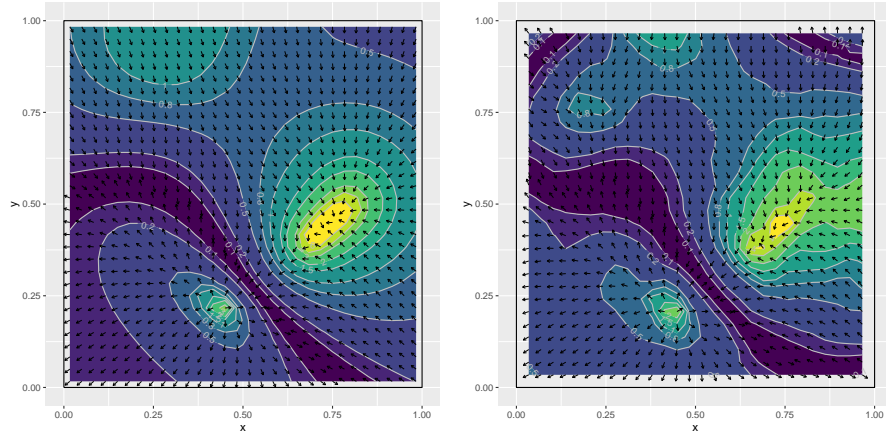
In this section, we show a real application of our method to model the spread and velocities of an infectious disease. In particular, we use the locations of COVID-19 infected individuals in Cali, one of the largest and most populated cities in Colombia. Data were provided by the Cali Municipal Public Health Secretary [Municipal Public Health Secretary of Cali,] and have confirmed locations of 208,551 infected individuals from 2020-03-01 to 2022-04-25. To begin, the geographical coordinates of the data were converted to UTM coordinates, and the values in the map are presented in meters. To model the LGCP, we construct a triangulated mesh covering the study region, in this case, the city boundary of Cali, Colombia. Once we have fitted the model, we make predictions in a grid with cells equally spaced 300 meters apart, which results in 1085 cells inside the city limits. For the temporal component, for simplicity, we use the 80 first days. In the image 7, we present the location of infected people on 4 different days in Cali, Colombia.

5.1 Intensity function

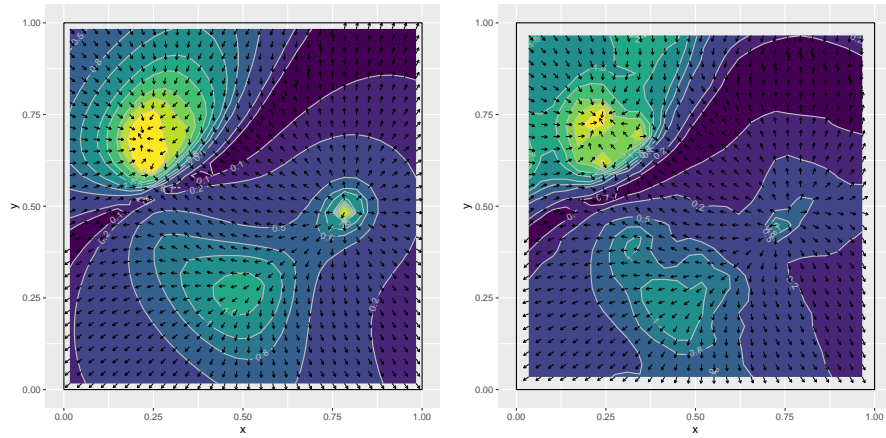
Following the ideas of Section 3.1, we apply a LGCP model with intensity function decomposed as the product of the spatial $\eta(\mathbf{u})$, temporal $\mu(t)$, and a residual spatio-temporal variation $\exp(\zeta(\mathbf{u}, t))$ as follows

$$\Lambda(\mathbf{u}, t) = \eta(\mathbf{u}) \cdot \mu(t) \cdot \exp(\zeta(\mathbf{u}, t)). \quad (16)$$

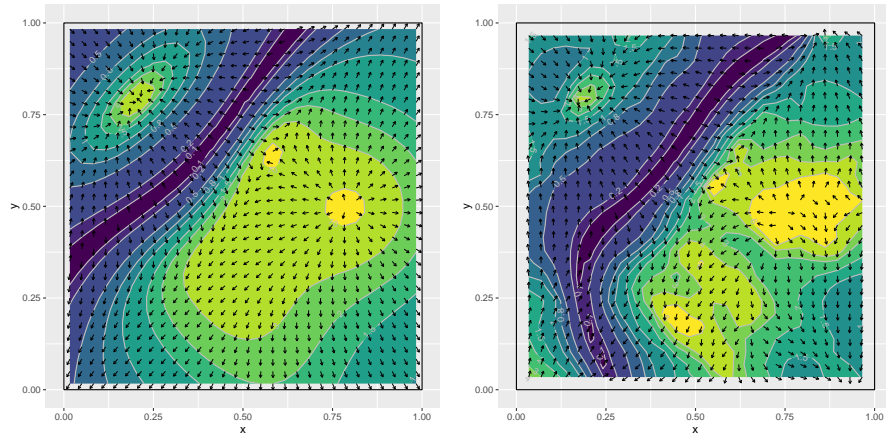
In practice, this decomposition requires first computing the spatial and temporal components separately and then using this information as an offset to compute the spatio-temporal component. The computation of each component is detailed below.



(a) $t = 0.225$



(b) $t = 0.575$



(c) $t = 0.875$

Figure 6: True minimum velocity of the intensity function (left) and finite difference approximation of this for the time points 0.225, 0.575, and 0.875. The arrows presented show the slowest speed of change and the direction of this speed is obtained and is positive.

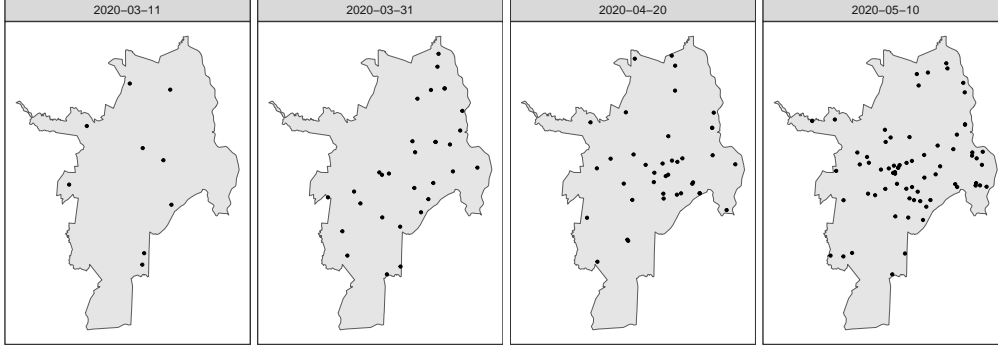


Figure 7: Locations of infected people in Cali, Colombia, for the days 2020-03-11, 2020-03-31, 2020-04-20 and 2020-05-10.

The spatial component represents the expected number of infected individuals in the city of Cali. To estimate this, we consider as a study region the city boundary of Cali. We use the R-INLA package to construct a triangulated mesh in this region, and compute the expected number of events using the dual mesh, which comprises a series of polygons surrounding each vertex of the original mesh [Moraga, 2023]. On the other hand, we obtain the population density in Cali from WorldPop, an open-access tool for population data. In this case, we used a resolution of 100×100 m cells defined in a square region that includes Cali (Figure 8). Then, the expected number of events in each polygon of the dual mesh is computed as the area of the polygon multiplied by the average population of the cells in that polygon [Krainski et al., 2018].

To estimate the temporal component representing the daily expected number of infected people, we use a spline model as explained in Section 3.1.1. The selected basis is related to the structure of the data. It takes into account first the day-of-week effects, periodical effects described by sine and cosine functions called Fourier basis, and finally an overall rising trend over the time captured by polynomial structure. The selected number of basis in each case was related to the simplicity and explainability of the model. In summary, the model has the following form

$$\log(\mu(t)) = \delta_{d_i} + \sum_{k=1}^3 (\alpha_k \cos \zeta(k\omega t) + \beta_k \sin(k\omega t) + \gamma_k t^k),$$

where $\omega = 2\pi/365$ is the annual periodicity. The estimators for the day-of-week effects are

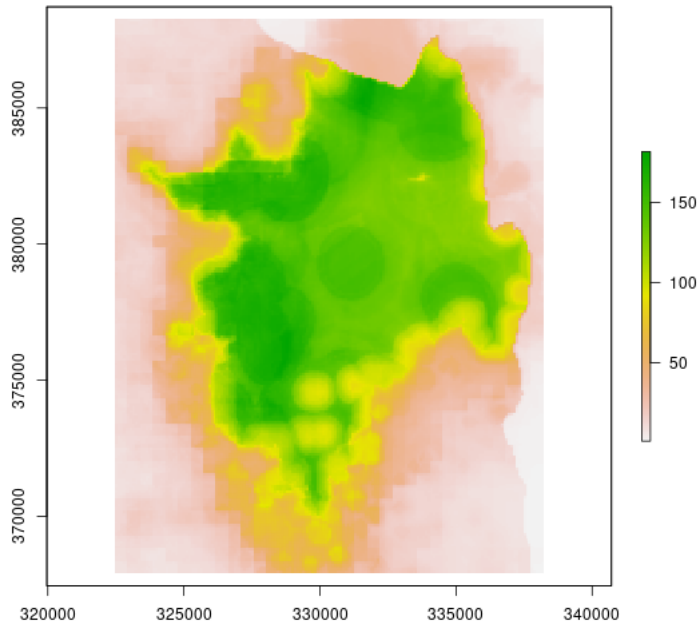


Figure 8: Population density in Cali, Colombia.

$\delta_d = \{-4.52, -4.58, -4.64, -4.60, -4.62, -4.70, -4.86\}$, where d_1 is Sunday, d_2 is Monday, etc. In addition, the estimators of the Fourier basis are $\alpha = \{3.59, 0.63, 0.34\}$, and $\beta = \{-18.71, -2.46, -0.50\}$. Finally, estimators for the polynomial basis for degrees $k = 1, 2, 3$ are $\gamma = \{0.69, -0.004, 8.31e - 06\}$. Figure 9 compares the result of the fitted model and the daily cases observed.

Finally, using the spatial and temporal components previously estimated as an offset, we estimate the parameters of the spatio-temporal random effect $\zeta(\mathbf{u}, t)$ and obtain an estimate for the posterior distribution of the intensity function $\lambda(\mathbf{u}, t)$. In Figure 10, we present the posterior mean of the intensity function for three different days.

5.2 Velocities

With the approximation of the intensity function, we can estimate the velocity and its direction using Equations (13), and (15) in the spatial domain. In Figures (11) and (12), we can see the estimate of the absolute value of the temporal derivative in (a), the estimate

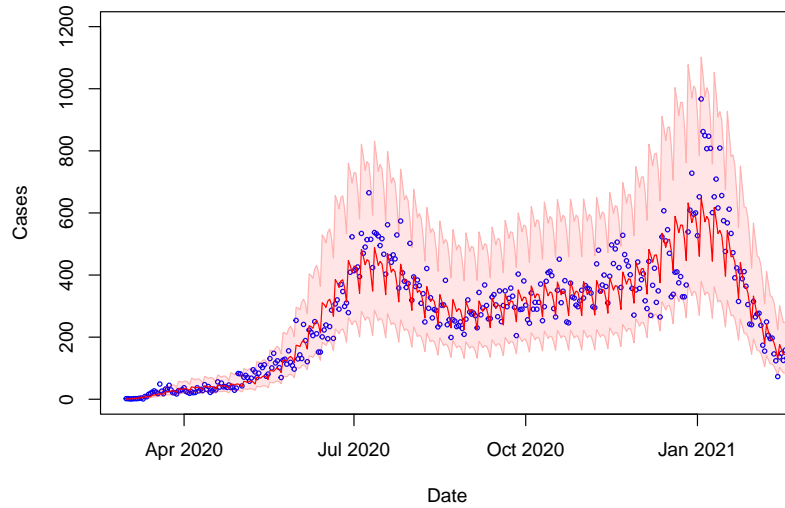


Figure 9: Total number of daily COVID-19 cases (blue dots) are presented with the fitted model (solid red line) and the confidence interval of the prediction over time (pink hatched area).

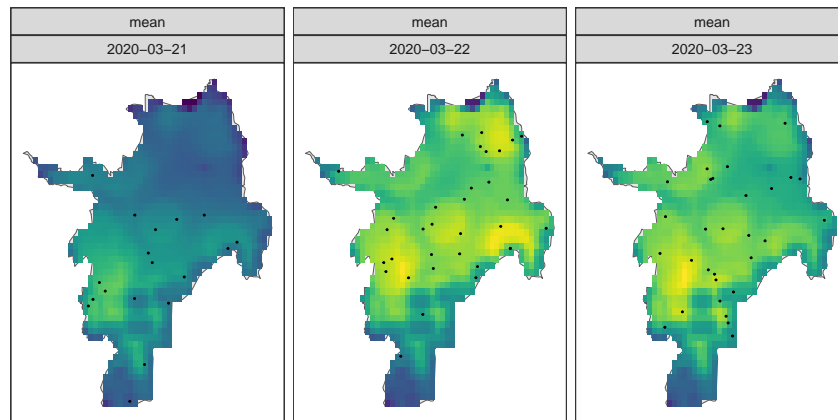


Figure 10: Posterior mean of the intensity function for the dates 2020-03-21, 2020-03-22, and 2020-03-23. Black dots are the locations of infected people on these days.

of the norm of the spatial gradient in (b), and the estimated minimum velocity in (c) for times 2020-03-22 and 2020-03-23 respectively. We presented these two approximations and the velocity (quotient of those two) because we want to show that large values of minimal velocities imply, at the same time, large values of the absolute value of the temporal

derivative and lower values of the norm of the spatial gradient.

Specifically, in Figure (11), we can see that in (a) and (b) in the upper right part of the map, there is a large magnitude of the absolute value of the temporal derivative, as well as a lower value of the norm of the gradient. Considering that, it is expected to see a hot spot in the same location as it showed in Figure 11 (c); also, notice the arrows are pointing to the hot spot. This hot spot shows the occurrence of new cases on day 2020-03-22 in the upper right part of Cali, which were not there the day before, as shown in Figure 10. Notice that, as we mentioned before, the arrows point to the hot spot, which means the number of cases in this zone is increasing.

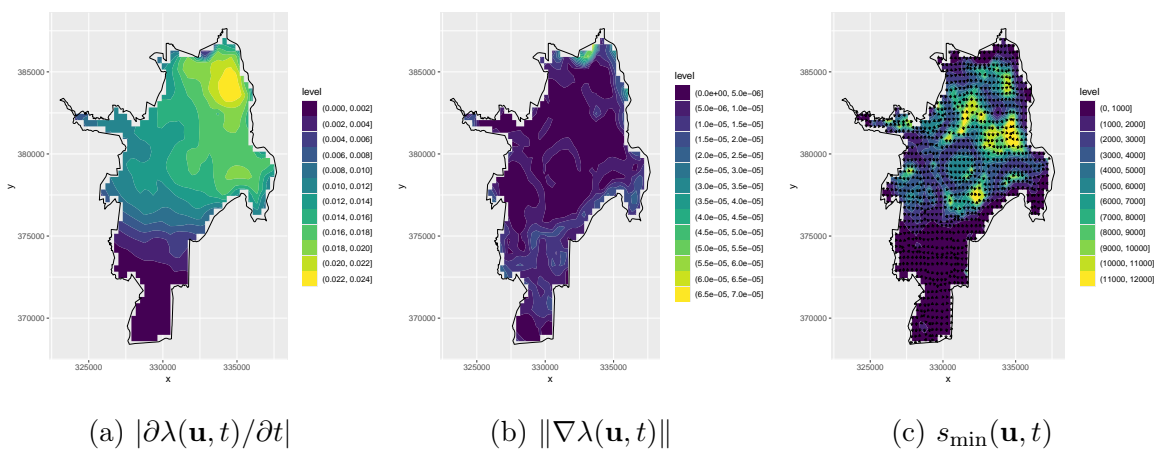


Figure 11: Velocity estimation in 2020-03-22.

On the other hand, in Figure 12 (a) and (b), we can see in the lower center of the map a significant value of the absolute value of the temporal derivative, but also a large value of the spatial gradient in the same location. That means that the value of the minimal velocity near this zone will not be as big as we expected; instead, it will be low compared to the other values, as we can see in Figure 12 (c). This happens because despite this zone presents new occurrences in comparison to the day before, as is shown in Figure 10, the density population of Cali is very narrow in that zone, and that will keep the minimal velocity smaller as is shown in Figure 8.

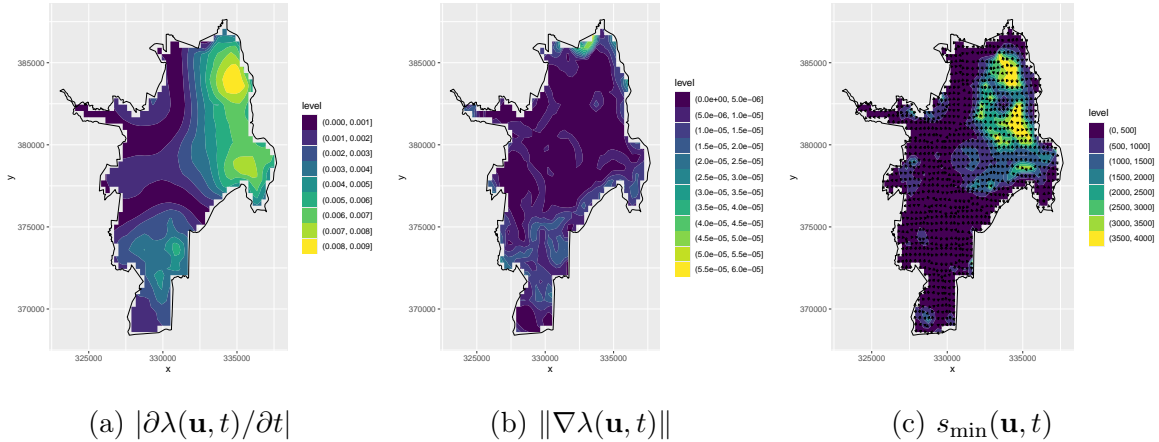


Figure 12: Velocity estimation in 2020-03-23.

6 Conclusions and discussion

In this paper, we present an alternative derivation of the formula for the minimal velocity based on the advection-diffuse equation for a sufficiently smooth function. We use that derivation as a starting point to extend it to the intensity function of a spatio-temporal point process. We use an LGCP model and consider a multiplicative decomposition of the space-time intensity function into spatial, temporal, and residual spatio-temporal components. First, the spatial component representing the expected number of cases can be estimated using a nonparametric estimation by kernels or integrating population data. Second, we proposed a spline model for the temporal component that uses day-of-week, periodic, and polynomial growing effects. Finally, for the spatio-temporal component, we used Matérn covariance structure on space and an independent structure over time. For inference, we used R-INLA and used the estimation of the intensity function to propose an approximation of the minimal velocity using finite differences.

Through a simulation study, we demonstrated that this approach works well, with the approximation by finite differences showing an overall good fit. That happens because the point approximation of the intensity function is smooth enough, which is one of the advantages of approximating an LGCP using basis functions in R-INLA. One of the main contributions of the velocity approximation proposed here is that we are not using a closed form of the covariance structure or a parametric estimation of the spatial or temporal

gradients. Here, we proposed a model-free approximation of the velocity that is flexible enough to capture *instantaneous* change in the intensity function between two time steps in the time resolution given by the data, for instance, the change of an infectious disease from one day to the other. We use first-order approximations of the partial derivatives in space and time mainly because of their simplicity. However, for future work, we can improve the approximation by using the smoothing properties of the intensity function to propose second-order approximations of the partial derivatives.

We also presented an application of COVID-19 data in Cali, Colombia, to demonstrate how this methodology works with real data. In this application, we can observe how the minimal velocity could help us understand how the disease spreads from one day to another. This application led us to think of a possible extension of this work. For example, we could model the interaction of more than one infectious disease in the same population, for instance, the evolution of dengue and chikungunya in a specific region [Pavani et al., 2023]. This approach could be extended to understand the marginal spread of each disease, considering their interactions.

In summary, we presented a method to approximate the minimal velocity and direction of disease spread using finite differences of the intensity function modeled with a spatio-temporal process. This is a data-driven approach that uses a flexible model that could be applied in infectious diseases or other spatio-temporal point patterns such as crime data or species locations, taking into account that the covariance structure for these problems is not the same as in contagious diseases.

References

- [Baddeley et al., 2015] Baddeley, A., Rubak, E., and Turner, R. (2015). *Spatial Point Patterns: Methodology and Applications with R*. Chapman and Hall/CRC Press, London.
- [Banerjee and Gelfand, 2003] Banerjee, S. and Gelfand, A. (2003). On smoothness properties of spatial processes. *Journal of Multivariate Analysis*, 84(1):85–100.
- [Bondarenko et al., 2020] Bondarenko, M., Kerr, D., Sorichetta, A., and Tatem (2020). Census/projection-disaggregated gridded population datasets for 189 countries in 2020 using built-settlement growth model (bsgm) outputs.
- [Diggle et al., 2005] Diggle, P., Rowlingson, B., and Su, T.-l. (2005). Point process methodology for on-line spatio-temporal disease surveillance. *Environmetrics*, 16(5):423–434.
- [Diggle et al., 2013] Diggle, P. J., Moraga, P., Rowlingson, B., and Taylor, B. M. (2013). Spatial and Spatio-Temporal Log-Gaussian Cox Processes: Extending the Geostatistical Paradigm. *Statistical Science*, 28(4):542 – 563.
- [González and Moraga, 2023] González, J. A. and Moraga, P. (2023). Non-parametric analysis of spatial and spatio-temporal point patterns. *The R Journal*, 15(1):65–82.
- [Kaye et al., 2020] Kaye, A., Okeagu, C., Pham, A., Silva, R., Hurley, J., Arron, B., Sarfraz, N., Lee, H., Ghali, G., Gamble, J., Liu, H., Urman, R., and Cornett, E. (2020). Economic impact of covid-19 pandemic on healthcare facilities and systems: International perspectives. *Best Practice and Research Clinical Anaesthesiology*, 35.
- [Krański et al., 2018] Krański, E., Gómez Rubio, V., Bakka, H., Lenzi, A., Castro-Camilo, D., Simpson, D., Lindgren, F., and Rue, H. (2018). *Advanced Spatial Modeling with Stochastic Partial Differential Equations Using R and INLA*. Chapman and Hall/CRC Press.
- [Matérn, 1960] Matérn, B. (1960). *Spatial variation: Stochastic models and their application to some problems in forest surveys and other sampling investigations*. Statens Skogsforskningsinstitut, Stockholm. Meddelanden Fran Statens Skogsforskningsinstitut, Band 49, Nr. 5.

- [Moraga, 2020] Moraga, P. (2020). Species distribution modeling using spatial point processes: a case study of sloth occurrence in costa rica. *The R Journal*, 12(2):293–310.
- [Moraga, 2023] Moraga, P. (2023). *Spatial Statistics for Data Science: Theory and Practice with R*. Chapman and Hall/CRC Press.
- [Municipal Public Health Secretary of Cali,] Municipal Public Health Secretary of Cali, M. C. <https://www.cali.gov.co/salud/>. Accessed: 2024-06-26.
- [Møller et al., 1998] Møller, J., Syversveen, A. R., and Waagepetersen, R. P. (1998). Log gaussian cox processes. *Scandinavian Journal of Statistics*, 25(3):451–482.
- [Pavani et al., 2023] Pavani, J., Bastos, L. S., and Moraga, P. (2023). Joint spatial modeling of the risks of co-circulating mosquito-borne diseases in ceará, brazil. *Spatial and Spatio-temporal Epidemiology*, 47:100616.
- [Quick et al., 2015] Quick, H., Banerjee, S., and Carlin, B. P. (2015). Bayesian modeling and analysis for gradients in spatiotemporal processes. *Biometrics*, 71(3):575–584.
- [Ribeiro Amaral et al., 2023] Ribeiro Amaral, A. V., Gonzalez, J. A., and Moraga, P. (2023). Spatio-temporal modeling of infectious diseases by integrating compartment and point process models. *Stochastic Environmental Research and Risk Assessment*, 37(4):1519–1533.
- [Rue et al., 2009] Rue, H., Martino, S., and Chopin, N. (2009). Approximate bayesian inference for latent gaussian models by using integrated nested laplace approximations. *Journal of the Royal Statistical Society: Series B (Statistical Methodology)*, 71(2):319–392.
- [Schliep et al., 2015] Schliep, E., Gelfand, A., and Clark, J. (2015). Stochastic modeling for velocity of climate change. *Journal of Agricultural, Biological, and Environmental Statistics*, 20:323–342.
- [Schliep and Gelfand, 2019] Schliep, E. M. and Gelfand, A. E. (2019). Velocities for spatio-temporal point patterns. *Spatial Statistics*, 29:204–225.

- [Sethian, 1999] Sethian, J. A. (1999). *Level Set Methods and Fast Marching Methods: Evolving Interfaces in Computational Geometry, Fluid Mechanics, Computer Vision, and Materials Science*. Cambridge Monograph on Applied and Computational Mathematics. Cambridge University Press, second edition.
- [Simpson et al., 2015] Simpson, D., Illian, J., Lindgren, F., Sørbye, S., and Rue, H. (2015). Going off grid: Computationally efficient inference for log-gaussian cox processes.
- [Terres and Gelfand, 2016] Terres, M. A. and Gelfand, A. E. (2016). Spatial process gradients and their use in sensitivity analysis for environmental processes. *Journal of Statistical Planning and Inference*, 168:106–119.
- [Wood, 2017] Wood, S. (2017). *Generalized Additive Models: An Introduction with R*. CRC Press, United States, 2 edition.
- [Wu et al., 2021] Wu, T., Jia, X., Shi, H., Niu, J., Yin, X., Xie, J., and Wang, X. (2021). Prevalence of mental health problems during the covid-19 pandemic: A systematic review and meta-analysis. *Journal of Affective Disorders*, 281:91–98.